HOKKAIDO UNIVERSITY

Title	Tomographic reconstruction of picosecond acoustic strain propagation
Author(s)	Tomoda, Motonobu; Matsuda, Osamu; Wright, Oliver B. et al.
Citation	Applied Physics Letters, 90(041114) https://doi.org/10.1063/1.2432238
Issue Date	2007-01-22
Doc URL	https://hdl.handle.net/2115/17178
Rights	Copyright © 2007 American Institute of Physics
Type	journal article
File Information	APL_90_041114.pdf

Tomographic reconstruction of picosecond acoustic strain propagation

Motonobu Tomoda,[a] Osamu Matsuda, and Oliver B. Wright
Department of Applied Physics, Graduate School of Engineering, Hokkaido University, Sapporo 060-8628, Japan

Roberto Li Voti
Dipartimento di Energetica, Università degli Studi di Roma "La Sapienza," Via A. Scarpa 14, 00161 Roma, Italy

By means of an ultrafast optical technique, picosecond acoustic strain pulses in a transparent medium are tomographically visualized. The authors reconstruct strain pulses in Au-coated glass from time-domain reflectivity changes as a function of the optical angle of incidence, with ~1 ps temporal and ~100 nm spatial resolutions. © *2007 American Institute of Physics.*
[DOI: 10.1063/1.2432238]

Laser picosecond acoustics is well adapted to the investigation of thin films and nanostructures.[1–5] Subpicosecond light pulses are typically used to generate and detect ~10–1000 GHz longitudinal acoustic strain pulses. The acoustic strain pulse shape depends on the optoacoustic generation and the acoustic propagation, related, respectively, to the electron and phonon scattering mechanisms.[1,4,6,7] Measuring the strain pulse shape is therefore useful for studying these mechanisms. In some materials it is possible to measure the strain pulse shape near a free surface by monitoring either surface displacements through beam deflection or changes in the phase of the optical reflectance.[2,8] However, no existing method can continuously monitor picosecond strain pulse shapes during propagation. Stimulated by progress in lower frequency acoustic tomography,[9] we present a method to achieve this.

Our sample consists of a thin metal film (with complex dielectric constant ε_2) deposited on a transparent substrate (with real ε_1), both materials being isotropic. For s-polarized probe light incidence at angle θ from the substrate side, the optical amplitude reflection coefficient r_0 (also termed the optical reflectance) can be expressed as[10]

$$r_0 = \frac{\cos\theta - \sqrt{\varepsilon_2/\varepsilon_1 - \sin^2\theta}}{\cos\theta + \sqrt{\varepsilon_2/\varepsilon_1 - \sin^2\theta}}. \qquad (1)$$

If ε_1 is slightly perturbed by a (anisotropic) longitudinal strain distribution $\eta_{33}(z,t)$ (~10^{-5} here) in the depth (z) direction, the reflectance is changed:[11–13]

$$\frac{\delta r_0}{r_0} = i\frac{\pi P_{12}}{\sqrt{\varepsilon_1}\lambda\cos\theta}\int_0^\infty \eta_{33}(z,t)\left[\exp\left(-i\frac{2\pi\sqrt{\varepsilon_1}z\cos\theta}{\lambda}\right)\right.$$
$$\left.+ r_0\exp\left(i\frac{2\pi\sqrt{\varepsilon_1}z\cos\theta}{\lambda}\right)\right]^2 dz, \qquad (2)$$

where variations in ε_2 and the effect of the finite substrate thickness have been ignored. Here, λ is the (central) wavelength of the probe light, P_{12} ($=\partial\varepsilon_1/\partial\eta_{33}$) is a photoelastic constant, and $z=0$ at the 1-2 interface. Equation (2), which generalizes the formula derived in the past for reflectance changes at normal incidence,[1,11] is an example of an inhomo-

geneous Fredholm integral.[14] We calculate $\eta_{33}(z,t)$ in the transparent substrate at a given time t from the observed reflectivity variation $\delta R_0/R_0 = 2\,\mathrm{Re}(\delta r_0/r_0)$ as a function of θ by solving the inverse problem (where $R_0 = |r_0|^2$).[14,15] (A similar approach involving optical phase variations should be feasible.)

A polished 10 mm radius hemisphere of BK7 glass, whose flat surface is coated with a thin polycrystalline Au film of thickness of 600 nm, is mounted on a rotation stage to set θ (see Fig. 1). A photodetector is mounted on a separate coaxial rotation stage set to 2θ. Visible s-polarized pump light pulses of duration of ~100 fs, repetition rate of 82 MHz, wavelength of 415 nm, and pulse energy of 1.1 nJ from the second harmonic of a Ti:sapphire mode-locked laser are used to illuminate an ~20 μm diameter [full width at half maximum (FWHM) intensity at $\theta=0°$] spot on the center of the flat Au-coated face of the hemisphere from the air side. This produces a maximum temperature rise of ~20 °C (in Au) after pump pulse arrival and a maximum steady state rise of ~110 °C at the BK7-Au interface in the pump beam spot. (After optical absorption to a depth $\zeta=18$ nm, electron diffusion distributes the initial temperature rise to depths of ~10 ζ.[4,16]) The thermoelastically generated acoustic strain

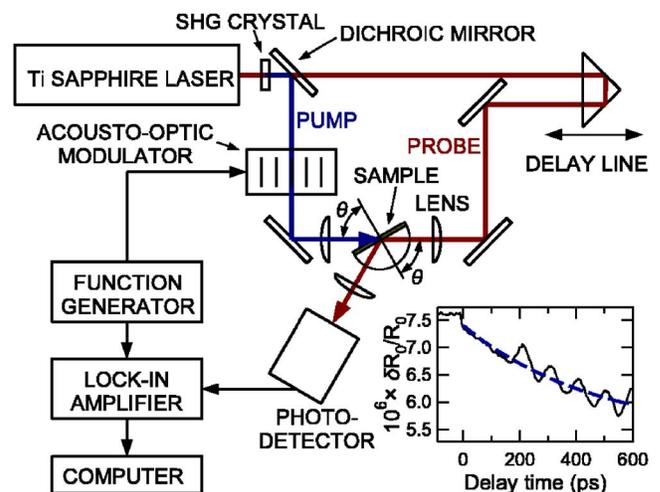

FIG. 1. (Color online) Experimental setup. Inset: relative reflectivity change for $\theta=60°$ (solid line) and exponential fit to thermoreflectance (dashed line). SHG: second-harmonic generation crystal.

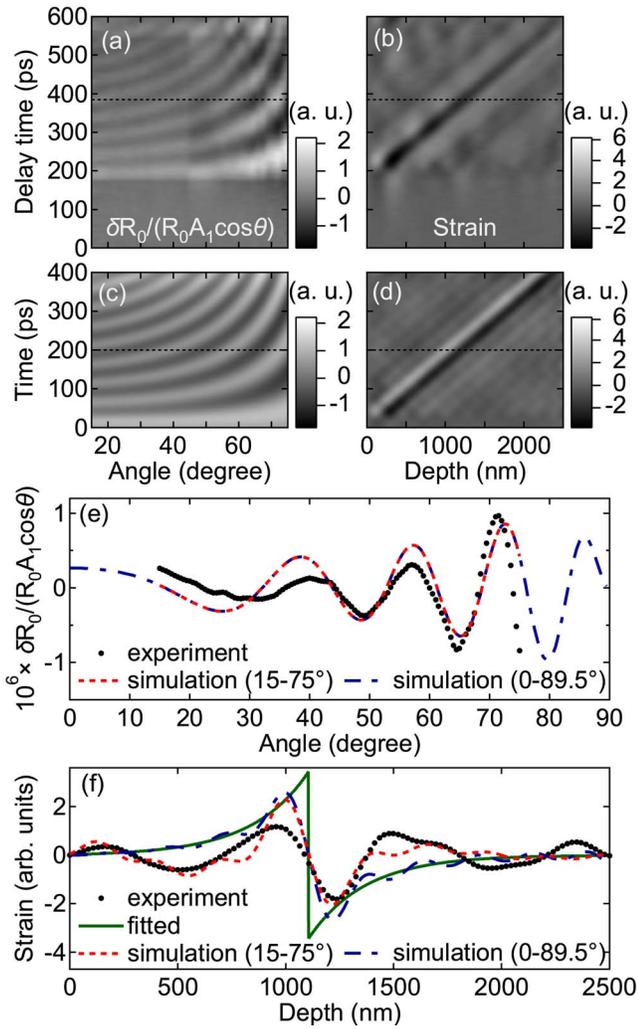[a] Electronic mail: mtomoda@eng.hokudai.ac.jp

FIG. 2. (Color online) (a) Density plot of the measured relative reflectivity variation $\delta R_0/R_0$, normalized by $A_1 \cos \theta$. (b) Experimentally reconstructed strain $\eta_{33}(z,t)$. (c) Simulated $\delta R_0(t)/R_0$ (for constant absorbed fluence). (d) Theoretically reconstructed $\eta_{33}(z,t)$. (e) $\delta R_0/(R_0 A_1 \cos \theta)$ at 385 ps vs angle θ. (f) Reconstructed strain distributions at $t=385$ ps. In (e) and (f) the dots are experimental data, the dashed lines are fits using the same range of θ as in experiment, and the dotted-dashed lines are fits using angles 0°–89.5°.
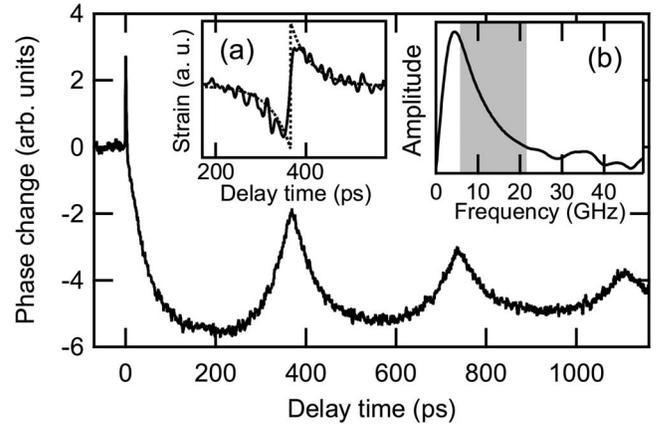

FIG. 3. Optical phase change measured interferometrically, showing multiple acoustic echoes. Inset (a): time derivative of the phase change, proportional to the acoustic strain pulse shape for the first echo. Dotted line: fit. Inset (b): Fourier spectrum of the strain in (a). The shaded range corresponds to the angle-scanned experiment.

pulses are bipolar in shape, with an amplitude of $\sim 10^{-5}$, duration of ~ 100 ps, spatial extent of ~ 300 nm (in Au), and with frequency components of up to ~ 10 GHz.[4] Infrared ($\lambda = 830$ nm) s-polarized probe pulses pass through an optical delay line and are focused to an ~ 10 μm diameter (FWHM intensity at $\theta = 0°$) spot on the Au film from the substrate side. $\delta R_0/R_0$ is monitored at the photodetector as a function of θ (in the range of 15–75°) and the pump-probe delay time t. By chopping the pump beam at 2 MHz and using lock-in detection, we track $\delta R_0(t)/R_0$ ($\sim 10^{-5}$). Both optical beams are incident at angle θ; the optical spots are thus ellipses with the same aspect ratio, whose horizontal sizes depend on θ.

The inset in Fig. 1 shows data for $\delta R_0(t)/R_0$ at $\theta = 60°$. At $t = 185$ ps the center of the strain pulse generated in the Au arrives at the Au-BK7 interface (i.e., when $t = d/v_2$, where $d = 600$ nm and $v_2 = 3360$ m s^{-1} are the Au film thickness and longitudinal sound velocity[17]). $\delta R_0(t)/R_0$ then oscillates owing to the photoelastic effect: the strain pulse acts as a moving mirror, producing oscillations by interference between the probe light reflected from the Au and from the

strain pulse.[3] The period is $\tau = \lambda/(2n_1 v_1 \cos \theta) \approx 94$ ps for $\theta = 60°$ and $n_1 = \sqrt{\varepsilon_1} = 1.51$ (the refractive index of BK7),[18] where $v_1 = 5860 \pm 30$ m s^{-1} is the derived longitudinal sound velocity of BK7 (from a range of θ values), close to the literature value.[18] [In fact if $\eta_{33}(z,t) = \eta_{33}(z - v_1 t)$, one can show that Eq. (2) contains a term proportional to $(C/\cos \theta)\cos(2\pi t/\tau + \phi_0)$, where C and ϕ_0 are constants for given materials and λ.] On transmission to the BK7 the acoustic strain pulse length increases by a factor of $v_1/v_2 = 1.75$.

The background thermoreflectance variation is subtracted by fitting to an exponential function (the dashed line in Fig. 1 inset). The data are then divided by $A_1 \cos \theta$ to account for the variation with θ of the absorbed pump fluence (arising in part from the elongation of the elliptical pump spot as θ increases), where $A_1(\theta) = 1 - R_1(\theta)$ is calculated from the pump beam reflectivity R_1 using known optical constants.[16] The increase in the (elliptical) probe spot area with θ ensures that the relative sizes of the pump and probe spots remain constant. Figure 2(a) shows a resulting density plot, corresponding to 116 different angles: 15°–20° in steps of 1°, and 20.5°–75° in steps of 0.5°. Angles $<15°$ or $>75°$ are precluded by lens overlap. The expected increase in τ with θ is clearly seen. Some random and systematic noise owing to slight optical alignment errors are evident.[19] A cross section of these data at delay time $t = 385$ ps is shown by the dots in Fig. 2(e).

In order to find $\eta_{33}(z,t)$, the whole θ-t data set was processed by the singular value decomposition method,[14,15,20] yielding a set of singular functions with an optimized eigenvalue number $N = 12$. The diagonal line in Fig. 2(b) shows the resulting reconstructed strain pulse $\eta_{33}(z,t)$, taking ε_1 from the literature.[16] We derive $v_1 = 5870 \pm 10$ m s^{-1} from these data (consistent with v_1 above). A cross section of these data at time $t = 385$ ps is shown by the dots in Fig. 2(f).

We have used a separate technique to determine $\eta_{33}(z,t)$ in the Au: a Sagnac interferometer measures the outward displacement $u(t)$ of the free surface of the Au film through optical phase changes $\delta\phi(t)$ under identical optical excitation conditions.[8,21] The acoustic strain pulse in the Au varies $\propto -du(t)/dt$.[2,8] $\delta\phi(t)$ is shown in Fig. 3, characterized by several echoes decaying in height according to the acoustic

strain reflection coefficient (~0.6) at the Au/BK7 interface. The temporal derivative of the first echo is shown in the inset (a). Because of the relatively small ultrasonic attenuation in polycrystalline Au and in silica at the acoustic frequencies (~10 GHz) and propagation distances (<3 μm) in question,[4,22] we directly compare this bipolar pulse shape with the acoustic strain pulse shape measured tomographically, accounting for the above-mentioned factor of v_1/v_2 =1.75.[23] The dotted line in the inset (a) of Fig. 3 is a fit to the measured strain pulse in the Au based on exponential tails [in the form $\text{sgn}(t')\exp(-v_2|t'|/L)$, where $L=150$ nm and $t'=t-t_0$, where t_0 corresponds to the center of the strain pulse]. The equivalent strain pulse in the BK7 in the spatial domain [in the form $-\text{sgn}(z')\exp(-|z'|/l)$, where $l=(v_1/v_2)L$ =260 nm and $z'=v_1t'$] is shown by the solid line in Fig. 2(f). Compared with the tomographic reconstruction, this strain pulse is significantly sharper.

To pin down the reasons for this we first plot in Fig. 2(c) the prediction for $\delta R_0(\theta,t)/R_0$ (at constant absorbed fluence), calculated from Eq. (2) using a *single* fitted strain pulse (appropriate for our temporal range $t<600$ ps). The time origin corresponds to the strain pulse arrival at the Au-BK7 interface ($t=185$ ps). A cross section corresponding to $t=385$ ps in experiment is shown by the dashed line in Fig. 2(e), giving reasonable agreement with experiment. The corresponding reconstructed $\eta_{33}(z,t)$ for $\theta=15°-75°$ is shown in Fig. 2(d), and a cross section at $t=385$ ps is shown by the dashed line in Fig. 2(f) (for $N=14$). The resulting strain pulse shape is similar to the experimental one. We have also plotted by the dotted-dashed lines in Figs. 2(e) and 2(f) the predictions corresponding to the angle range of 0°–89.5° (for $N=18$). The reconstruction is only slightly improved by this.

These findings can be understood by considering the constraints on the reconstructed acoustic frequencies. A measurement at angle θ is sensitive to an acoustic strain Fourier component at a frequency $f=1/\tau=(2n_1v_1\cos\theta)/\lambda$; our measurements for angles 15°–75° correspond to the limited range of 5.5–20.7 GHz, as shown by the shaded region in the inset (b) of Fig. 3 together with the temporal Fourier transform of the interferometrically measured strain pulse. For angles 0°–89.5°, this frequency range broadens to 0.2–22 GHz. It is primarily the frequency range that limits the reconstruction in our case. Apart from noise reduction, the best way to improve our reconstruction fidelity would therefore be to increase the maximum frequency f by reducing the optical wavelength λ (or by using a λ scan involving smaller λ).

Our reconstruction method also relies on the use of literature values of optical constants to correct for the $A_1(\theta)$ variation. Ideally this measurement should be done experimentally. Another experimental limitation is the possible walk-off between the strain distribution and the obliquely incident optical probe beam in the substrate as the strain penetrates deeper. We have made quantitative estimates of this effect by taking the cross correlation of the probe beam and strain pulse lateral distributions. In the present experiment this effect should only decrease the signal by a maximum of 8% at $t=600$ ps and $\theta=75°$.

The spatial resolution in the present study is limited to ~100 nm, but it should be possible to improve on this using a shorter optical probe wavelength. The method could be extended to reconstruct other fields that couple to the dielectric constant, such as carrier or temperature distributions or nonlinear optical pulse propagation, in transparent or semitransparent materials.

[1]C. Thomsen, H. T. Grahn, H. J. Maris, and J. Tauc, Phys. Rev. B **34**, 4129 (1986).
[2]O. B. Wright and K. Kawashima, Phys. Rev. Lett. **69**, 1668 (1992).
[3]H.-N. Lin, R. J. Stoner, H. J. Maris, and J. Tauc, J. Appl. Phys. **69**, 3816 (1991).
[4]O. B. Wright, Phys. Rev. B **49**, 9985 (1994).
[5]C. Rossignol and B. Perrin, IEEE Trans. Ultrason. Ferroelectr. Freq. Control **52**, 1354 (2005).
[6]G. Tas and H. J. Maris, Phys. Rev. B **49**, 15046 (1994).
[7]O. B. Wright, B. Perrin, O. Matsuda, and V. E. Gusev, Phys. Rev. B **64**, 081202 (2001).
[8]D. H. Hurley and O. B. Wright, Opt. Lett. **24**, 1305 (1999).
[9]P. Gren, S. Schedin, and X. Li, Appl. Opt. **37**, 834 (1998).
[10]B. E. A. Saleh and M. C. Teich, *Fundamentals of Photonics* (Wiley, New York, 1991), p. 205.
[11]O. Matsuda and O. B. Wright, J. Opt. Soc. Am. B **19**, 3028 (2002).
[12]O. Matsuda and O. B. Wright, Rev. Sci. Instrum. **74**, 895 (2003).
[13]O. Matsuda and O. B. Wright (unpublished).
[14]J. F. Power, Rev. Sci. Instrum. **73**, 4057 (2002).
[15]C. Glorieux, R. Li Voti, J. Thoen, M. Bertolotti, and C. Sibilia, Inverse Probl. **15**, 1149 (1999).
[16]E. D. Palik, *Handbook of Optical Constants* (Academic, New York, 1985), Vol. I, p. 294.
[17]O. L. Anderson, in *Physical Acoustics*, edited by W. P. Mason (Academic, New York, 1965), Vol. 3B, p. 43.
[18]See http://www.ispoptics.com/new_webpage/opt_mat_specs.htm
[19]The pump and probe spot overlap was optimized for each angle, and the photodetector position was readjusted for $\theta>45°$.
[20]R. Li Voti, C. Sibilia, and M. Bertolotti, Int. J. Thermophys. **26**, 1833 (2005).
[21]T. Tachizaki, T. Muroya, O. Matsuda, Y. Sugawara, D. H. Hurley, and O. B. Wright, Rev. Sci. Instrum. **77**, 043713 (2006).
[22]T. C. Zhu, H. J. Maris, and J. Tauc, Phys. Rev. B **44**, 4281 (1991).
[23]Because of the limitation on spatial resolution in the reconstructed strain pulses, the effects of ultrasonic attenuation were not included in the numerical modeling.